HEAT GENERATION DURING PLUNGE STAGE IN FRICTION STIR WELDING

by

Darko M. VELJIĆ [a*], Marko P. RAKIN [b], Milenko M, PEROVIĆ [c], Bojan I. MEDJO [b], Zoran J. RADAKOVIĆ [d], Petar M. TODOROVIĆ [e], and Mirko N. PAVIŠIĆ [d]

[a] IHIS Science & Technology, Zemun, Belgrade, Serbia
[b] Faculty of Technology and Metallurgy, University of Belgrade, Belgrade, Serbia
[c] Chamber of Economy of Montenegro, Podgorica, Montenegro
[d] Faculty of Mechanical Engineering, University of Belgrade, Belgrade, Serbia
[e] Faculty of Engineering, University of Kragujevac, Kragujevac, Serbia

Original scientific paper
DOI: 10.2298/TSCI120301205V

This paper deals with the heat generation in the Al alloy Al2024-T3 plate under different rotating speeds and plunge speeds during the plunge stage of friction stir welding. A 3-D finite element model is developed in the commercial code ABAQUS/Explicit using the arbitrary Lagrangian-Eulerian formulation, the Johnson-Cook material law, and Coulomb's Law of friction. The heat generation in friction stir welding can be divided into two parts: frictional heat generated by the tool and heat generated by material deformation near the pin and the tool shoulder region. Numerical results obtained in this work indicate a more prominent influence from the friction-generated heat. The slip rate of the tool relative to the workpiece material is related to this portion of heat. The material velocity, on the other hand, is related to the heat generated by plastic deformation. Increasing the plunging speed of the tool decreases the friction-generated heat and increases the amount of deformation-generated heat, while increasing the tool rotating speed has the opposite influence on both heat portions. Numerical results are compared with the experimental ones, in order to validate the numerical model, and a good agreement is obtained.

Key words: *friction stir welding, numerical simulation, temperature fields, heat generation, friction, plastic strain, slip rate*

Introduction

Friction stir welding (FSW) is a robust solid state joining process that was introduced by The Welding Institute in early nineties, the last century. It is primarily a two-stage process: a plunge welding stage and a linear welding stage, as shown in fig. 1. In the plunge stage, a hard non-consumable rotating tool penetrates the plates to be welded. In the linear welding phase, the tool moves along the joint line [1]. During this process, the tool rotation creates conditions for the generation of energy by friction between the tool and the workpiece, as well as through the plastic deformation of the material. Both energies heat the plates, enabling their joining at temperatures lower than the melting point of the material.

A number of publications dealing with numerical investigations of welding [2, 3] and FSW process can be found in the literature [4-12]. For example, Zhang *et al*., [4], and Zhang and

* Corresponding author; e-mail: veljic.darko@gmail.com

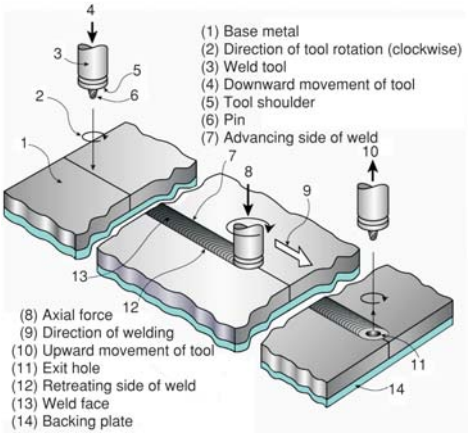

Figure 1. Schematic illustration of FSW process [14]

Zhang [5] carried out semi-coupled thermo-mechanical finite element analyses of the FSW process and the associated microstructural changes. In several references, the main objective was to examine the effect of various FSW process parameters (including tool design) on the heat/mass transport processes [5-7]). Song and Kovačević [8] and Chen and Kovačević [9-10] presented numerical thermo-mechanical modeling of FSW for both similar and dissimilar joints. Some simplified analyses can also be found, such as Dong *et al*. [11], where several models were developed to separately deal with the thermal and mechanical aspects of the FSW.

In majority of the literature, the emphasis is on the simulation of the welding process, *i. e*. the linear welding phase, while plunge stage is rarely examined [1, 12, 13]. However, plunging is a vital phase of the FSW process, because it creates the initial thermo-mechanical conditions in the material, *i. e*. conditions prior to the start of the linear welding phase. Also, numerical modeling of the plunging process is very demanding due to the pronounced mesh distortion under the pin. This paper compares the numerical results of the temperature change during the plunge stage of the FSW with the experimental data obtained by thermal imaging. Numerical modeling is also used for analysis of the heat generation (by friction and material deformation) during this stage.

Table 1. The chemical composition of the base material [15]

Alloy	Content of element, [wt%]							
	Cu	Mg	Mn	Fe	Si	Zn	Ti	Al
2024-T3	4.80	1.41	0.72	0.28	0.13	0.07	0.15	bal.

Table 2. Material properties of Al 2024 T351 [14-15]

Material properties	Value
Young's modulus of elastic. [GPa]	73.1
Poisson's ratio	0.33
Initial yield stress [MPa]	345
Ultimate tensile strength [MPa]	483
Thermal conductivity [$W\mu^{-1}K^{-1}$]	121
Coefficient of thermal expansion [$°C^{-1}$]	$24.7 \cdot 10^{-6}$
Density [kgm^{-3}]	2770
Specific heat capacity [$Jk^{-1}g°C^{-1}$]	875
Solidus [°C]	502
Liquidus [°C]	638

Experiment

One of the goals of the experimental investigations was tracking the temperature changes on the top surface of the workpiece in the vicinity of the tool shoulder periphery during the plunge stage of the FSW process. The sheets' dimensions were $180 \times 65 \times 3$ mm; they were produced from a high-strength Al alloy 2024 T3. Table 1 shows the chemical composition of the base material. The thermal and mechanical properties used for the numerical model are given in tab. 2 [14-17].

The experiment was performed on a CNC milling machine, produced by Prvomajska, type AG400, 12 kW. A tool manufactured from Cr-V-Mo tool steel (56NiCrMoV7) was used; the tool had concentric circles on the tool shoulder and left-hand thread on

the tool pin. The tool hardness after thermal treatment (quenched and tempered condition) was 54 HRC. The material of the backing plate is steel 42CrMo4.

The temperature change during the welding process was registered with a thermovision camera FLIR system, ThermaCAM P640. The measurement range of the camera was from –40 to 2000 °C, with an accuracy of ±2 °C. High-quality pictures were produced using the new generation detector. ThermaCAM Quick Report 1.1 software was used for processing the recorded data from the camera and creating the diagrams of the time-dependence of the temperature on the top surface of the workpiece in the vicinity of the tool shoulder periphery.

Figure 2 shows the process of plunging the tool into the workpiece. The values of the FSW parameters were:

– Specimen 1 – tool rotation speed n = 400 rpm, tool plunge speed v = 0.0405 mm/s, and
– Specimen 2 – tool rotation speed n = 447 rpm, tool plunge speed v = 0.0405 mm/s.

Figure 2. Plunge stage of FSW

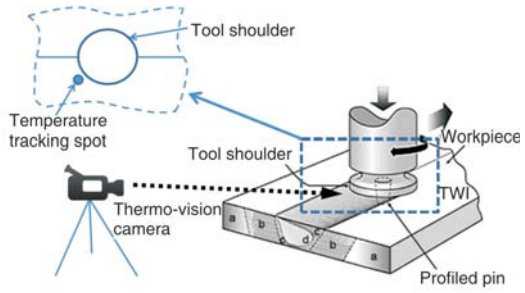

Figure 3. Schematic view of the experimental set-up

Schematic view of the experimental set-up is given in fig. 3. The exact position of the temperature tracking spot, used for comparison with numerical results, is shown in fig. 3 (left) – see also fig. 6.

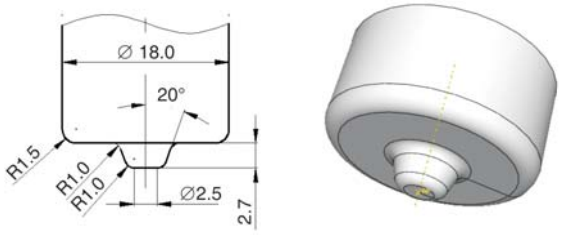

Figure 4. The welding tool used in numerical analysis

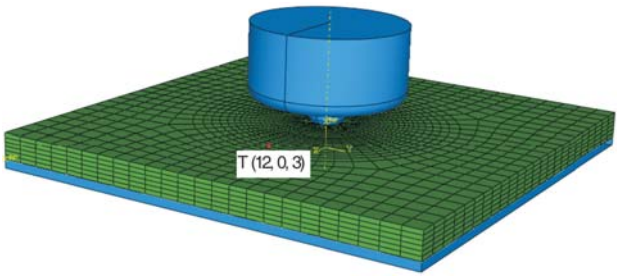

Figure 5. Numerical model of the welding plate, tool, and backing plate, with the co-ordinates of the point for measuring the time-dependence of the temperature

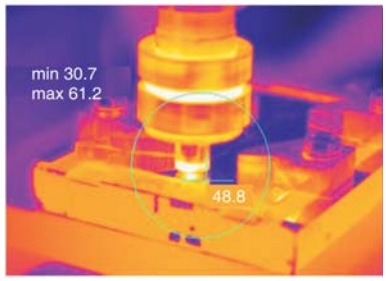

Figure 6. Thermal image recorded after 12 seconds, Specimen 1 v = 0.0405 mm/s, n = 400 rpm

Numerical model

The dimensions of the welding plate in the 3-D numerical model are 50 × 50 × 3 mm. The model consists of thermo-mechanically coupled hexahedral finite elements with 8-nodes (C3D8RT [18]), each having trilinear displacement and temperature degrees of freedom. This element produces uniform strain (first-order reduced integration) and contains hourglass control [18, 19].

The mesh consisted of 15.276 nodes and 12.800 elements. The tool and the backing plate are modeled as rigid bodies having no thermal degrees of freedom. The main tool geometry in the finite element model is simplified and does not include the thread, because this would lead to excessive mesh distortion. The numerical model of the welding plate, tool and backing plate is shown in figs. 4 and 5.

Johnson-Cook elastic-plastic model

A temperature and strain rate dependent material law (elastic-plastic Johnson-Cook law) is implemented [14]:

$$\sigma_y = [A + B(\varepsilon_p)^n]\left[1 + C\left(\frac{\dot{\varepsilon}_p}{\dot{\varepsilon}_o}\right)\right]\left[1 - \left(\frac{T - T_{\text{room}}}{T_{\text{melt}} - T_{\text{room}}}\right)^m\right] \tag{1}$$

where $T_{\text{melt}} = 502$ °C is the melting point or solidus temperature, $T_{\text{room}} = 20$ °C – the ambient temperature, T [°C] – the effective temperature, $A = 369$ MPa, $B = 684$ MPa, $n = 0.73$, $m = 1.7$, and $C = 0.0083$. A, B, C, n, and m are material/test constants for the Johnson-Cook strain rate dependent yield stress for Al 2024 T3 [17].

Thermal model

The governing equation for heat transfer during the FSW process can be written as:

$$\rho c = \frac{\partial T}{\partial t} = \frac{\partial}{\partial x}\left[k_x \frac{\partial T}{\partial x}\right] + \frac{\partial}{\partial y}\left[k_y \frac{\partial T}{\partial y}\right] + \frac{\partial}{\partial z}\left[k_z \frac{\partial T}{\partial z}\right] + \dot{q}_p \tag{2}$$

where ρ is the density, c – the specific heat, k – the heat conductivity, T – the temperature, t – the time, $\dot{q}_p$ – the heat generation coming from plastic energy dissipation due to shear deformation, and x, y, and z are the spatial co-ordinates [20]. The rate of heat generation due to plastic energy dissipation, $\dot{q}_p$ is computed from:

$$\dot{q}_p = \eta \tau \dot{\varepsilon}^{\text{pl}} \tag{3}$$

where η is the factor of conversion of mechanical to thermal energy (0.9) [21], τ – the shear stress, and $\dot{\varepsilon}^{\text{pl}}$ – the plastic strain rate. Frictional heat generation between tool and workpieces can be written as:

$$\dot{q}_{\text{f}} = \mu p \dot{\gamma} \tag{4}$$

where $\dot{q}_{\text{f}}$ is the frictional heat generation, μ – the coefficient of friction, p – the pressure, and $\dot{\gamma}$ – the slip rate.

The heat transfer through the bottom surface of the workpiece is controlled by the heat transfer coefficient of 3000 W/m^{2}K [20]. A constant friction coefficient of 0.3 is assumed between the tool and the workpiece and the penalty contact method is used to model the contact interaction between the two surfaces. Heat convection coefficients on the surface of the workpiece are $h = 10$ W/m^{2}K with the ambient temperature of 20 °C [21].

Results and discussion

Figure 9 shows the temperature field recorded by the thermo-vision camera in the 12th second after the beginning of the plunge stage at the fusion line, Specimen 1. The cross marks the location on the surface of the workpiece for tracking the temperature changes during the welding process. This point is located in the vicinity of the tool shoulder periphery (*i. e.* it is the point on the top surface of the workpiece, at a distance of 12 mm from the tool symmetry axis).

Comparison of the numerically and experimentally obtained results of the time-dependence of the temperature during the plunge stage is shown in fig. 7 (Specimens 1 and 2). Bearing in mind that the welding of the two specimens is performed with a small intermediate time, the clamping tools were heated, which also caused a mild pre-heating of the plates during their fixation. This fact did not influence the test results; hence, the initial temperature for the numerical model was 25 °C in all cases. In the first 40 seconds of the plunge stage, the experimentally obtained temperature increases more slowly in comparison with the numerical results. The reason for this increase is that the left-hand thread of the tool pin caused the appearance of the "drill effect". However, from the moment contact between the tool shoulder and the plates is established, the difference between the numerically and experimentally determined values becomes negligible. This can be attributed to the more prominent influence of the tool shoulder in the heat generation process, when compared with the less prominent influence of the tool pin.

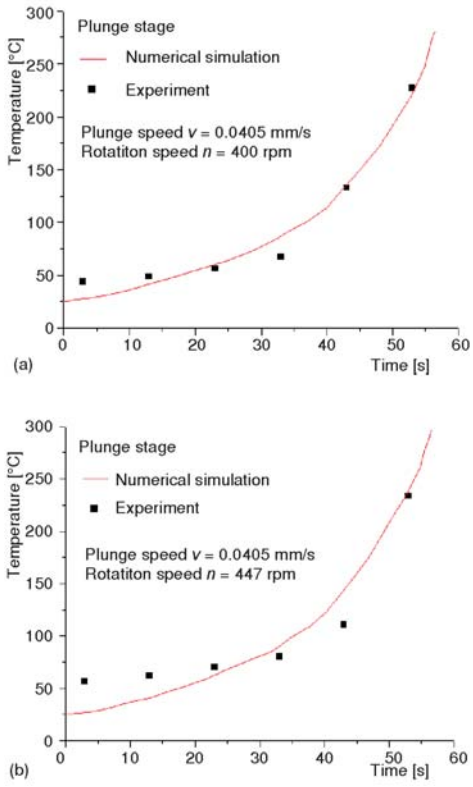

Figure 7. The time-dependence of the temperature for (a) v = 0.0405 mm/s, n = 400 rpm, and for (b) v = 0.0405 mm/s, n = 447 rpm

The distributions of the tool slip rate relative to the welded material are shown in fig. 8. Maximum slip rates are always located in the periphery of the contact surface between the tool shoulder and the material, because the material is less intensively heated in this area and the circumferential speed value is the largest. This figure shows that the slip rate in the area close to the tool pin is significantly lower, because the material is very hot and the circumferential speed is smaller. The slip rate is directly related to the amount of friction-generated heat (eq. 4).

Unlike the slip rate, the material velocity is lowest at the periphery of the tool shoulder. In the area near the pin, the flow of the material is very prominent due to the high temperatures (*i. e.* small values of the shearing yield stress). As the material "adheres" to the tool shoulder, maximum velocities of the material are more likely to appear in the area with higher circumferential speeds, as shown in fig. 9. The material velocity is related to the heat generation due to the plastic deformation (eq. 3).

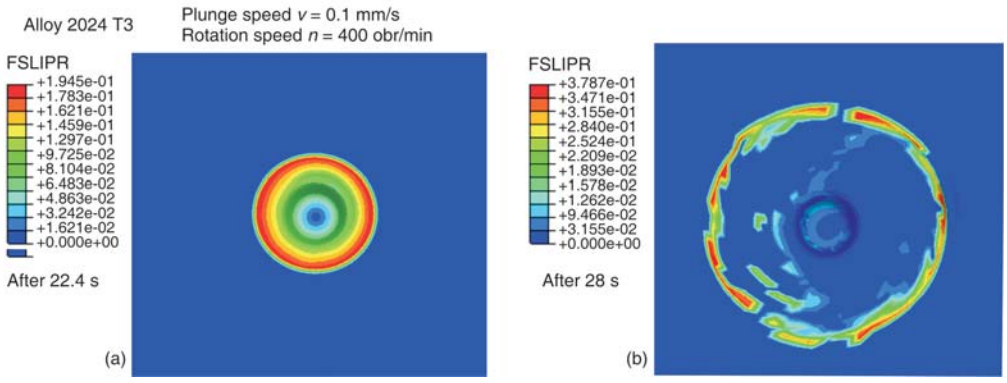

Figure 8. Slip rate distributions before (a) and after (b) the establishment of the contact between the tool shoulder and the material (for color image see journal web site**)**

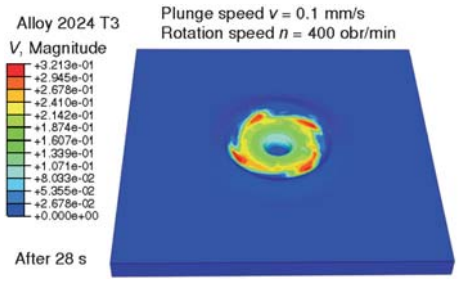

Figure 9. The velocity field
(for color image see journal web site**)**

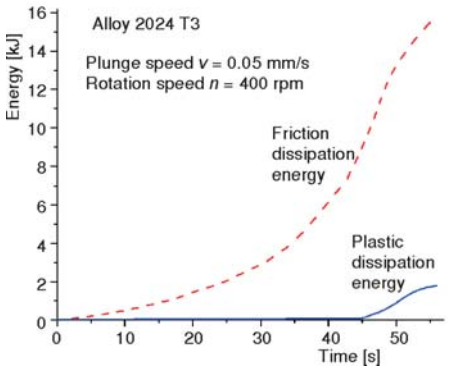

Figure 10. Time-dependence of the energy dissipation

The results of the simulation of the plunge stage indicate that the largest portion of the generated heat is the result of the friction between the tool and the workpiece. For the case with the plunge speed v = 0.05 mm/s and n = 400 rpm, the friction-generated heat is 15.9 kJ, and the deformation-generated heat is 1.8 kJ (fig. 10). Therefore, the total amount of the generated heat during plunging is 17.7 kJ. Such a large percentage of the heat caused by friction (89.83%) can be attributed to large slip rates on the workpiece surface, due to the large values of the tool rotation speed and pressure force.

As shown in fig. 10, the friction-generated heat is significantly increased after 40 s, when the contact between the tool shoulder and the material is first established. The heat caused by plastic deformation significantly increases after 45 s, because the plastic deformation is the most prominent when the previously mentioned contact between the tool shoulder and material has been established, right before the end of the plunge stage.

Figure 11 shows the amount of heat generated by friction for different tool rotation speeds. The plunge speed is 0.1 mm/s. Increasing the tool rotation speed increases the amount of heat generated by friction. Note that this component of the generated heat suddenly increases after 22 s, when the contact between the workpiece and the tool shoulder has been established.

Similar conclusions regarding the change of frictional dissipation energy with the change of the rotation speed was obtained by Awang and Mucino [22] in a recent study, for friction stir spot welding (FSSW) of Al 6061-T6. This type of FSW does not include translation of

the tool, and is therefore used for comparison with plunge stage here, having in mind that majority of the literature neglects the simulation of the plunge stage.

Comparison of the plastic dissipation energies for three different tool rotation speeds is given in fig. 12. After 22 s, the contact between the tool shoulder and the material is established and the amount of generated heat suddenly increases; a similar jump was also obtained in [22] for FSSW of Al 6061-T6. For the lower rotation speeds (300 rpm), the tool shoulder contacts the extruded material later; hence, a sudden energy increase occurs 1 s later in this case. From these results, it can also be concluded that lower tool rotation speeds cause more intensive heat generation due to plastic deformation. This can be explained by the lower temperature in the welding zone – the resistance to deformation is more prominent, which in turn causes the increase in deformation-generated heat. The percentage of this portion of heat in the entire heat amount is 18-25%. If these values are compared with fig.10, it can be concluded that increasing the plunging speed increases the relative amount of the heat generated by plastic deformation.

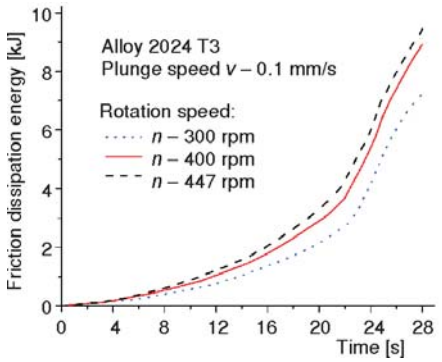

Figure 11. Frictional dissipation energy for three different rotation speeds

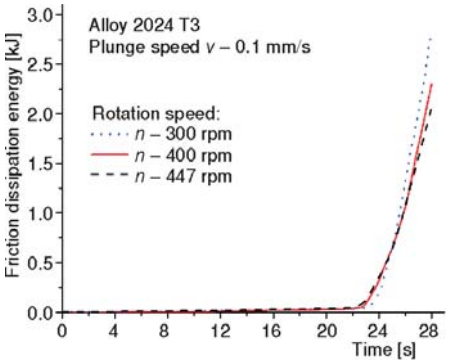

Figure 12. Plastic dissipation energy for three different rotation speeds

Conclusions

The main conclusions obtained in this study can be summarized as follows.

- A good agreement of numerically and experimentally determined time-dependence of the temperature has been obtained.
- Workpiece (plate) temperature suddenly increases when the tool shoulder establishes contact with it.
- Slip rate is found to be directly related to the generated friction heat.
- Maximum values of the slip rate have been observed on the periphery of the plate – tool shoulder contact surface.
- The velocity of the material is related to the heat generated by the plastic deformation.
- The velocity of the material has the smallest values on the periphery of the tool shoulder.
- The amounts of heat generated by friction and plastic deformation suddenly increase after contact between the workpiece and the tool shoulder is established.
- The heat generated by friction between the workpiece and the tool can account for the largest percentage of the generated heat.
- Increasing the plunge speed decreases the amount of heat generated by friction and increases the heat generated by plastic strains.
- Increasing the tool rotation speed increases the amount of heat generated by friction and decreases the heat generated by plastic strains.

Acknowledgments

The authors acknowledge the support from the Serbian Ministry of Education, Science and Technological Development of the Republic of Serbia under the projects TR 34018, TR 34016 and TR 35006.

References

[1] Veljić, D., *et al*., Numerical Simulation of the Plunge Stage in Friction Stir Welding, *Structural Integrity and Life, 11* (2011), 2, pp. 131-134
[2] Ivanović, I., *et al*., Numerical Study of Transient Three-Dimensional Heat Conduction Problem with a Moving Heat Source, *Thermal Science, 15* (2011) 1, pp. 257-266
[3] Berković, M., *et al*., Analysis of Welded Joints by Applying the Finite Element Method, *Structural Integrity and Life, 4* (2004), 2, pp. 75-83
[4] Zhang, H. W., *et al*.,The Finite Element Simulation of the Friction Stir Welding Process, *Materials Science and Engineering A*, *403* (2005), 1-2, pp. 340-348
[5] Zhang, H. W., Zhang, Z., Numerical Modeling of Friction Stir Welding Process by Using Rate-Dependent Constitutive Model, *Journal of Materials Science & Technology, 23* (2007), 1, pp. 73-80
[6] Xu, S., *et al*., Finite Element Simulation of Material Flow in Friction Stir Welding, *Science and Technology of Welding and Joining, 6* (2001), 3, pp. 191-193
[7] Assidi, M., *et al*., Friction Model for Friction Stir Welding Process Simulation: Calibrations from Welding Experiments, *International Journal of Machine Tools & Manufacture, 50* (2010), 2, pp. 143-155
[8] Song, M., Kovačević, R., Numerical and Experimental Study of the Heat Transfer Process in Friction Stir Welding, *Journal of Engineering Manufacture, 217* (2003), 1, pp. 73-85
[9] Chen, C. M., Kovačević, R., Finite Element Modeling of Friction Stir Welding – Thermal and Thermomechanical Analysis, *International Journal of Machine Tools & Manufacture, 43* (2003), 13, pp. 1319-1326
[10] Chen, C. M., Kovačević, R., Joining of Al 6061 Alloy to AISI 1018 Steel by Combined Effects of Fusion and Solid State Welding, *International Journal of machine Tools and Manufacture, 44* (2004), 11, pp. 1205-1214
[11] Dong, P., *et al*., Coupled Thermomechanical Analysis of Friction Stir Welding Process Using Simplified Models, *Science and Technology of Welding and Joining, 6* (2001), 5, pp. 281-287
[12] Perović, M., *et al*., Friction-Stir Welding of High-Strength Aluminium Alloys and a Numerical Simulation of the Plunge Stage, *Materials and Technology, 46* (2012) 3, pp. 105-111
[13] Mandal, S., *et al*., Experimental and Numerical Investigation of the Plunge Stage in Friction Stir Welding, *Journal of Materials Processing Technology, 203* (2008), 1-3, pp. 411-419
[14] Veljić, D., *et al*., A Coupled Thermo-Mechanical Model of Friction Stir Welding, *Thermal Science, 16* (2012), 2 pp. 527-534
[15] ***, Certificate Conformity, ALCOA International, Inc., Approved Certificate, No. 47831, 1990
[16] ***, Aluminum 2024-T3 – ASM Material Data Sheet, http://asm.matweb.com/search/SpecificMaterial.asp?bassnum=MA2024T3
[17] Johnson, R. G., Cook, W. H., A Constitutive Model and Data for Metals Subjected to Large Strains, High Strain Rates and High Temperatures, *Proceedings*, 7th International Symposium on Ballistics, Hague, The Netherlands, 1983, pp. 541-547
[18] ***, Abaqus Inc., Analysis – User's Manual v.6.7, 2007
[19] Zhang, Z., *et al*., Effect of Traverse/Rotational Speed on Material Deformations and Temperature Distributions in Friction Stir Welding, *Journal of Materials Science & Technology, 24* (2008), 6, pp. 907-913
[20] Park, K., Development and Analysis of Ultrasonic Assisted Friction Stir Welding Process, Ph. D. thesis, University of Michigan, Ann Arbor, Mich., USA, 2009
[21] Schmidt, H., Hattel, J., A Local Model for the Thermomechanical Conditions in Friction Stir Welding, *Modelling and Simulation in Materials Science and Engineering, 13* (2005), 1, pp. 77-93
[22] Awang, M., Mucino, V., Energy Generation during Friction Stir Spot Welding (FSSW) of Al 6061-T6 Plates, *Materials and Manufacturing Processes, 25* (2010), 1, pp. 167-174

Paper submitted: March 1, 2012
Paper revised: June 12, 2012
Paper accepted: October 16, 2012